Spin polarized I-V characteristics and shot noise of Pt atomic wires

Bin Wang and Jian Wang*

Department of Physics and the Center of Theoretical and Computational Physics, The University of Hong Kong, Pokfulam Road, Hong Kong, China

(Received 23 June 2011; published 3 October 2011)

We report a first-principles investigation of spin polarized transport properties of Pt atomic chains in contact with two semi-infinite Pt slabs along the (111) direction. Our approach is based on the nonequilibrium Green's function coupled with density functional theory so that the Coulomb interaction is included in the calculation of current and shot noise on the Hartree level. For Pt atomic chains with different numbers of Pt atoms, we calculate the spin polarized I-V curve and shot noise. Our results show that the current increases almost linearly with bias for all Pt atomic structures. The calculated Fano factors are comparable to the recent experimental data and show sub-Poissonian behavior.

DOI: 10.1103/PhysRevB.84.165401 PACS number(s): 85.35.−p, 73.63.−b, 71.15.Mb

I. INTRODUCTION

Understanding the electronic behavior in atomic structures is the foundation of fabricating promising nanodevices. As the ultimate limit of a nanodevice, an atomic nanowire-based tunneling junction has attracted great attention in past decades because of the fundamentals of electric transport properties as well as the typical fabrication technologies.[1] Many atomic nanowires have been achieved using experimental techniques, such as mechanically controllable break junctions[2–5] and self-assembly on a solid surface.[6,7] Due to the reduction in dimension, atomic nanowires show interesting properties. For instance, quantized conductance has been observed in noble metal nanowires[2,8] and semiconductor nanowires,[9] where the conductance is almost the integral multiple of the conductance quantum $2e^2/h$. Theoretical investigation predicted that the conductance of an atomic junction oscillates with an increase in atom numbers,[10–12] which has been observed experimentally.[5,13] A reversible metal-insulator phase transition was observed in In atomic nanowire under low temperatures characterized by STM and reflection high-energy electron diffraction.[14] It was found that a small band gap appears at the zone boundary with a decrease in temperature, attributed to the backfolding of bands around the K point. Recently, several theoretical investigations have predicted that Pt atomic nanowires can be spin polarized and show ferromagnetic properties,[15–17] although the macroscopic Pt bulk is paramagnetic. Due to the strong ability of magnetization of unfilled 5d orbitals, the paramagnetic state of bulk Pt is expected to change to a ferromagnetic state considering the reduction in dimension with a concomitant increase in the density of states.[15,18]

Shot noise describes the fluctuation of current and is an intrinsic property of atomic structures due to the quantization of an electric charge of finite size. An important parameter to describe shot noise is the Fano factor F, which is defined as $F = S/2eI$, where S is the shot noise and I is the average current. Conventionally, when F is greater than 1, it is referred to as super-Poissonian shot noise; otherwise, the shot noise is sub-Poissonian. Shot noise is influenced by two factors: the Pauli exclusion principle and the Coulomb interaction. The former leads to a suppression of shot noise, and the latter contributes a suppression or an enhancement of shot noise.[19–21] The suppression of shot noise has been confirmed experimentally in quantum point contacts,[22,23] single-electron tunneling regimes,[24,25] graphene nanoribbons,[26,27] and atom-size metallic contacts.[28] The enhancement of shot noise was also observed in kinds of GaAs-based quantum contacts when the system is in the negative differential conductance region.[29,30] Theoretically, shot noise has been investigated extensively in mesoscopic systems.[31,32] For nanodevices, less attention has been focused on shot noise,[33,34] especially spin-dependent shot noise.

Recently, one experimental group measured the shot noise of Pt atomic nanowires using a controllable break junction method.[35] By analyzing the noise spectra, they concluded that the conducting transmission channels are unpolarized. This is really a surprising result because it is different from the previous theoretical investigations.[15–17]On the other hand, most previous investigations of the Pt nanowire focus on its electric transport properties under equilibrium,[15–17] while few works concentrate on its spin-dependent transport properties.[36] In this paper, we carry out first-principles calculations to investigate the spin polarized transport properties and shot noise of several Pt atomic nanowires with different numbers of atoms. Numerical results show that the I-V curve is approximately linear with the increase in bias voltage, and the magnitudes of the I-V curve for different Pt wires are comparable. For all structures and different bias voltages, the Fano factor shows sub-Poissonian behavior. The value of our Fano factor is also comparable to that in a recent experiment.[35] Although our numerical data on shot noise are consistent with those of experimental work, the conclusion we draw from our numerical results supports the prediction of previous theoretical investigations. Through analyzing the Fano factor of spin -polarized Pt tunneling junctions, we found that the surprising conclusion of the experiment that Pt atomic nanowire always shows nonmagnetic ground state is due to a mistake in analyzing the physics of the Fano factor.

II. THEORETICAL FORMALISM

For nanodevices with a size comparable to the phase relaxation length, the spin-dependent current can be calculated

by the Landauer-Büttiker formalism as follows:

$$I_\sigma = \frac{e}{h}\int d\epsilon [f_L(\epsilon) - f_R(\epsilon)]\mathrm{Tr}[T_\sigma(\epsilon)], \tag{1}$$

where $\sigma = \uparrow, \downarrow$ denotes different spin; f_L and f_R are the Fermi distribution functions of the left (L) and right (R) leads, respectively. The spin polarized transmission matrix T_σ is given by[37,38]

$$T_\sigma(\epsilon) = \int_{-\pi}^{\pi} \frac{dk_\parallel}{(2\pi)^2} T_\sigma(\epsilon, k_\parallel), \tag{2}$$

$$T_\sigma(\epsilon, k_\parallel) = \left[\Gamma_{L,k_\parallel} G^r_{k_\parallel} \Gamma_{R,k_\parallel} G^a_{k_\parallel}\right]_{\sigma\sigma}, \tag{3}$$

where $k_\parallel = (k_x, k_y)$ is the wave vector and is sampled in the two-dimensional (2D) Brillouin zone. Here $G^r_{k_\parallel}$ and $G^a_{k_\parallel}$ are the retarded and advanced Green's functions of the system at $k_\parallel$ with the size doubled due to the spin index; $\Gamma_{L,k_\parallel}$ ($\Gamma_{R,k_\parallel}$) is the linewidth function at $k_\parallel$, which describes the coupling between the left (right) lead and the scattering region. In terms of transmission eigenchannels, we have

$$I_\sigma = \frac{e}{h}\int d\epsilon [f_L(\epsilon) - f_R(\epsilon)] \sum_{n=1}^{N} \tau_{n,\sigma}(\epsilon), \tag{4}$$

where $\tau_{n,\sigma}$ is the nth eigenvalue of the transmission matrix T_σ, which describes the spin-dependent transmission coefficient in the nth eigenchannel, with maximum value 1, and $\sum_n$ is over all the eigenchannels.

The gauge-invariant formula of electric noise can be expressed as[21,39]

$$S_I = 2G_0 \sum_\sigma \int d\epsilon \mathrm{Tr}[T_\sigma][f_L(1-f_L) + f_R(1-f_R)] + 2G_0 \sum_\sigma \int d\epsilon \mathrm{Tr}[T_\sigma(1-T_\sigma)](f_L - f_R)^2, \tag{5}$$

where $G_0 = e^2/h$ is the conductance quantum. Note that the Green's function in T_σ has to be calculated self-consistently by the equations

$$G^r(\epsilon, U) = \frac{1}{\epsilon - H - U - \Sigma^r}, \tag{6}$$

where H includes the exchange and correlation potentials and the Coulomb potential U is obtained from the Poisson equation,

$$\nabla^2 U(x) = 4\pi i q \int (d\epsilon/2\pi) G^<(\epsilon, U), \tag{7}$$

and the lesser Green's function is related to the retarded and advanced Green's functions as

$$G^< = iG^r \sum_\beta \Gamma_\beta f_\beta G^a. \tag{8}$$

In terms of eigenchannels, Eq. (5) can be rewritten as

$$S_I = 2G_0 \int d\epsilon \sum_{n\sigma} \tau_{n\sigma}[f_L(1-f_L) + f_R(1-f_R)] + 2G_0 \int d\epsilon \sum_{n\sigma} \tau_{n\sigma}(1-\tau_{n\sigma})(f_L - f_R)^2. \tag{9}$$

In Eq. (9), the first term describes the noise spectrum due to the thermal electric emission and the second term originates from the finite bias voltage. In the equilibrium state with $V = 0$, the electric noise in Eq. (9) reduces to the thermal noise. In the low-temperature limit with $k_B T \ll eV$, the first term in Eq. (9) tends to 0 and S_I reduces to the so-called shot noise S as

$$S = 2G_0 \int d\epsilon \sum_{\sigma,n=1}^{N} \tau_{n,\sigma}(1-\tau_{n,\sigma}), \tag{10}$$

where the integral is over the energy range from $E_F + eV_L$ to $E_F + eV_R$, with $V = V_L - V_R$ the bias voltage and E_F the Fermi energy. The Fano factor F can be expressed as

$$F = \frac{\int d\epsilon \sum_{\sigma,n} \tau_{n,\sigma}(1-\tau_{n,\sigma})}{\int d\epsilon \sum_{\sigma,n} \tau_{n,\sigma}}. \tag{11}$$

At equilibrium, F reaches its maximum value of 1 when all transmission channels are closed, which corresponds to a Coulomb block. For a spin-degenerate system with N eigenchannels, where $\tau_{n,\uparrow} \equiv \tau_{n,\downarrow}$, F reaches a minimum value of 0 when $\tau_{n,\uparrow} = \tau_{n,\downarrow} = 1$ for each $n \leqslant N$, while for a spin-polarized system, F reduces to the minimum value of 0 when $\tau_{n,\sigma} = 1$ and $\tau_{n,\bar{\sigma}} = 0$ for all $n \leqslant N$. In this case, transport is ballistic and only electrons with spin σ are allowed to pass through the nanodevice. Beyond the equilibrium state, the Fano factor can increase drastically with an increase in bias voltage. In the negative differential resistance regime, the Fano factor can be larger than 1.[40] Experimentally, one can obtain information on electric transport for individual transmission channels by measuring the Fano factor of the nanodevice.[41,42]

III. STRUCTURE AND CALCULATION METHOD

The left inset in Fig. 1 shows the schematic structure of a Pt tunneling junction where a monowire with two Pt atoms

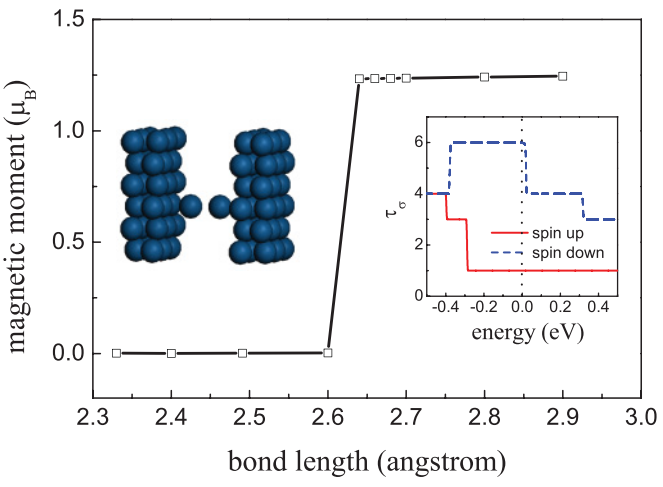

FIG. 1. (Color online) Magnetic moment per atom of an ideal periodic Pt wire as a function of the bond length d. Right inset: Transmission coefficient τ_σ versus energy of an ideal periodic Pt wire when $d = 2.8$ Å. The solid (red) line, dashed (blue) line, and dotted (black) line indicate the spin-up channel, spin-down channel, and Fermi level, respectively. Left inset: Schematic structure of a Pt tunneling junction where a Pt wire with two atoms is sandwiched between two semi-infinite Pt slabs.

is sandwiched between two semi-infinite Pt slabs along the (111) direction. Compared to the actual chemical structures, two assumptions are employed in our modeling junction of chemical bonding to facilitate the calculation. First, the distance between the wire tip and the Pt slab is supposed to be the same as the bond length of the monowire. Second, we ignored the contact deformation of the Pt slab, although some atoms may be slightly away from the Pt slab due to the string tension of atomic wire.[15] Experimentally, the length of atomic nanowires is controllable by adjusting the force on the break junctions. To obtain enough information to model the experimental result of Kumar*et al.*,[35] four structures of Pt tunneling junctions were investigated, with the number of atoms N in the monowires equal to 2, 3, 4, and 5.

To investigate the electric transport properties and noise spectra of Pt tunneling junctions, first-principles calculations were carried out within the nonequilibriun Green's function (NEGF) + density functional theory (DFT) using the transport package NANODCAL.[43,44] With this method, the system Hamiltonian as well as the charge distribution is obtained from DFT calculations, and spin polarized transport properties are determined by the NEGF. The LCAO fireball basis set is used to expand the initial electronic density. The standard norm-conserving pseudopotential[45] is employed to define the atomic cores and the exchange correlation is treated at the LSDA level.[46] To obtain accurate results, a double-ζ polarization LCAO basis including s, p, and d orbitals is used. The self-consistency is controlled by a numerical tolerance of 10^{-5} a.u.

Once we obtain the self-consistent Hamiltonian $H + U$ under a given bias voltage, we can obtain the Green's function $G^r_{k_\parallel}$ using Eq. (6). By substituting $G^r_{k_\parallel}$ into Eq. (3), we can calculate the spin polarized transmission matrix $T_\sigma(\epsilon)$ of the device according to Eq. (2). And then the spin-polarized current, shot noise, and Fano factor can be calculated using Eqs. (1), (10), and (11), respectively.

IV. NUMERICAL RESULTS

First, we investigated the electric properties of an ideal periodic Pt nanowire. Figure 1 shows the magnetic moment per atom of a Pt wire with an increase in bond length d. When $d < 2.6$ Å, the magnetic moment is almost equal to 0 and the nanowire is spin degenerate. When $d > 2.6$ Å, a nonzero magnetic moment appears and reaches a plateau with a value of about 1.24 μ_B. This value does not change with further increase in the bond length. This property has been illustrated in previous theoretical investigations[15,17] and explained by Zabala *et al.*[18] Due to the reduction in dimension accompanied by the appearance of a flat band, the Stoner stability criterion against magnetism is violated, which results in a spontaneous transition of magnetization of metal atomic wires when the flat band crosses the Fermi level.[18] This phase transition property is especially obvious for the transition metals with unfilled d orbitals.[15] The transmission coefficient τ_σ of a periodic Pt wire with $d = 2.8$ Å is shown in the right inset in Fig. 1. Obviously, the Pt wire is spin polarized and has six spin-down channels but only one spin-up channel around the Fermi level with $E_F = 0$. When the energy is higher than E_F, $\tau_\downarrow$ drops to 4 from 6, which indicates a d-type double-degenerate spin-down

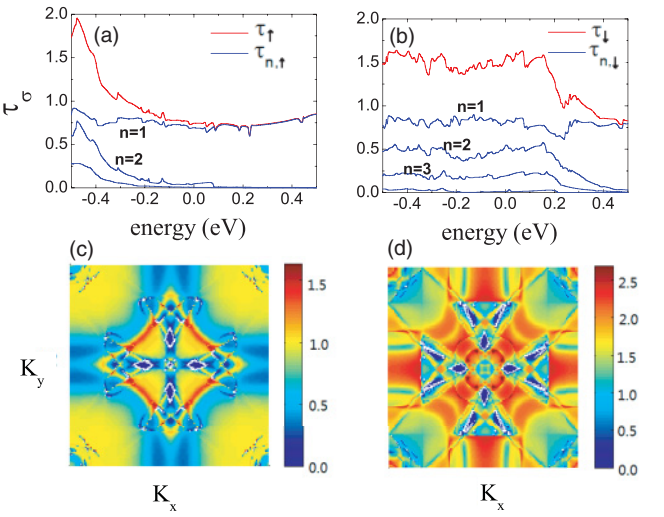

FIG. 2. (Color online) Spin-dependent transmission coefficient of a Pt tunneling junction with $N = 3$ under zero bias voltage. (a) $\tau_\uparrow$ and $\tau_{n,\uparrow}$ as a function of energy. (b) $\tau_\downarrow$ and $\tau_{n,\downarrow}$ as a function of energy. The Fermi level is shifted to 0 eV. (c) K sampling $\tau_\uparrow(k_\parallel)$ and (d) K sampling $\tau_\downarrow(k_\parallel)$ in the 2D Brillouin zone at the Fermi level.

flat band across the Fermi level.[16] In order to illustrate the main feature of noise spectra for spin-polarized systems, we fixed $d = 2.8$ Å for all the Pt tunneling junctions in the following investigation.

Figure 2 shows the transmission coefficient of a Pt tunneling junction with $N = 3$ (three Pt atoms) at zero bias voltage. Figure 2(a) shows $\tau_{n,\uparrow}$ and $\tau_\uparrow$, and Fig. 2(b) shows $\tau_{n,\downarrow}$ and $\tau_\downarrow$ as a function of energy. Due to the perfect contact, the Pt tunneling junction shows a comparatively flat transmission coefficient around the Fermi level for both spin-up and spin-down electrons, which is different from the numerical result in Ref. 17, where the resonant peak around the Fermi level comes from the sharp Pt contact.[17] For spin-up electrons, there are two eigenchannels which contribute to $\tau_\uparrow$ at the Fermi level, although there is only one spin-up channel for an ideal periodic Pt wire. This is not surprising since there are more incoming channels in the Pt slab. The total spin-up transmission coefficient $\tau_\uparrow = 0.8$, which is dominated by one of the eigenchannels with a contribution larger than 94%. For spin-down electrons, there are three eigenchannels around the Fermi level and $\tau_\downarrow = 1.55$. $\tau = \sum_\sigma \tau_\sigma$ is equal to 2.35, which is consistent with previous theoretical[16] and experimental[35] results where the conductance of the Pt junction is roughly from 2 G_0 to 4 G_0. Figures 2(c) and 2(d) plot the quantity $\tau_\sigma(k_\parallel)$ at the Fermi level in the 2D Brillouin zone with $\sigma = \uparrow$ and $\sigma = \downarrow$, respectively. For $\sigma = \uparrow$, the "hot spots," where $\tau_\sigma(k_\parallel)$ shows sharp resonance features corresponding to a high transport probability, are distributed symmetrically around the Γ point, which is mostly contributed by the s-type channel of the Pt wire. However, for $\sigma = \downarrow$, the resonant feature at various $k_\parallel$ values is much more complicated than that of a spin-up channel. The hot spots in the $\sigma = \downarrow$ panel is contributed by three resonant eigenchannels, each of which is a combination of one s-type and two pd-type orbitals.

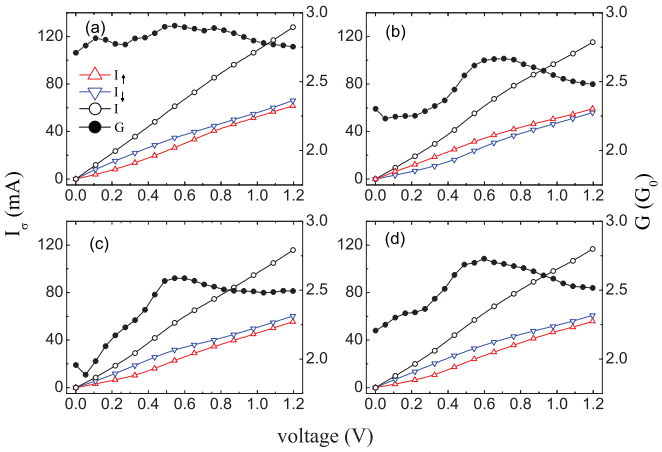

FIG. 3. (Color online) Spin polarized current I_σ and conductance G versus bias voltage of Pt tunneling junctions for (a) $N = 2$, (b) $N = 3$, (c) $N = 4$, and (d) $N = 5$. $I_\uparrow$, $I_\downarrow$, total current I, and conductance G are shown by the up triangle, down triangle, open circle, and filled circle lines, respectively.

Using Eq. (4), we calculated the spin polarized current I_σ of Pt tunneling junctions with $N = 2,3,4,5$ as shown in Fig. 3. For all structures, $I_\uparrow$ is always smaller than $I_\downarrow$ for all bias voltages. The total current I shows almost-linear behavior as a function of bias voltage. The linear behavior of the I-V curve is especially obvious for $N = 2$, where the conductance is almost a constant of $2.75G_0$ for all bias voltages. Hence it makes sense to talk about the average conductance $G = I/V$. For $N = 3,4,5$, the average conductances increase initially and then decrease around the average value of $2.5G_0$. For all structures, there are three spin-up channels and three spin-down channels contributing to the transmission coefficient. To analyze the contribution from each eigenchannel under different bias voltages, we projected the conductance G to each spin polarized eigenchannel. The eigenchannel conductance is defined as $G_{n,\sigma} = I_{n,\sigma}/V$, where $I_{n,\sigma} = \frac{e}{h}\int d\epsilon[f_L(\epsilon) - f_R(\epsilon)]\tau_{n,\sigma}(\epsilon)$. Figure 4 shows $G_{n,\sigma}$ as a function of bias voltage. For the structure with $N = 2$, $G_{2,\uparrow}$ and $G_{3,\uparrow}$ increase with the bias voltage, while $G_{1,\downarrow}$, $G_{2,\downarrow}$, and $G_{3,\downarrow}$ decrease with the bias voltage. As a consequence, the total conductance G is almost a constant as shown in Fig. 3(a).

The Fano factor versus voltage is shown in Fig. 5. For all the structures and different bias voltages, the Fano factors always show sub-Poissonian behavior where $F < 1$. With an increase in bias voltage, the Fano factor decreases initially and then increases, which is due to the competition among all $G_{n,\sigma}$ values under different bias voltages. Roughly speaking, a larger $G_{n,\sigma}$ gives a smaller contribution to F, which can be understood by Eq.(11). Here we show how the transmission channels contribute to the Fano factor. For the structure with $N = 2$, there are six eigen-channels that give $F = 0.316$ when $V = 0$ with $G_{1,\uparrow} = 0.7223$, $G_{2,\uparrow} = 0.1115$, $G_{3,\uparrow} = 0.0136$, $G_{1,\downarrow} = 0.8753$, $G_{2,\downarrow} = 0.7035$, and $G_{3,\downarrow} = 0.2592$.

In order to illustrate the main feature of noise spectra for spin polarized tunneling junctions, Fano factors versus conductance G under different bias voltages from 0 to 1.2 V are given in Fig. 6. From the definition of Fano

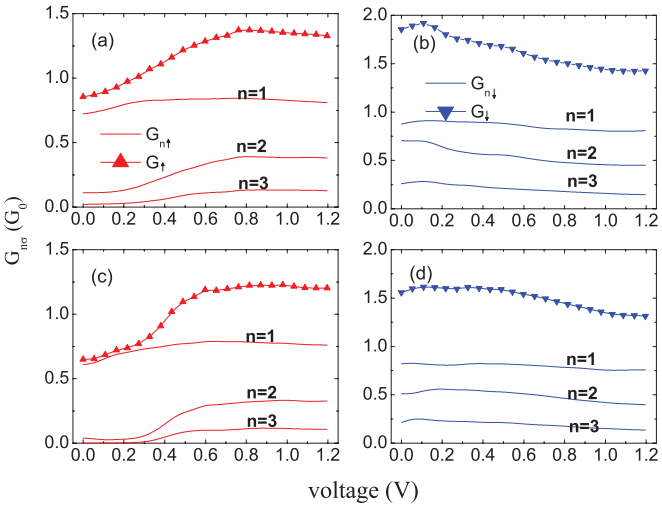

FIG. 4. (Color online) Eigen-channel conductance $G_{n,\sigma}$ versus bias voltage for (a) spin up channels of N = 2; (b) spin down channels of N = 2; (c) spin up channels of N = 5; (d) spin down channels of N = 5. The triangle line is the spin conductance G_σ contributed from all spin-polarized eigen-channels.

factor $F = \sum_i \tau_i(1-\tau_i)/\sum_i \tau_i$, it is easy to find that the maximum value of the Fano factor for a fixed conductance $G = \frac{e^2}{h}\sum_i \tau_i$ appears when τ_i is independent of i. Hence the line $F = 1 - G/N$ vs G gives the maximum for the Fano factor where N is the number of conducting channels. In Fig. 6, we use dotted lines to indicate the maximum value of F for four or six spin-degenerate eigenchannels. For the minimum value of Fano factor with a particular spin polarization (SP), there is no analytic solution. We have calculated it numerically and plot it in Fig. 6 for different SPs. For instance, the solid (red) line corresponds to the minimum value of F for unpolarized spin with an SP equal to 0 and the (black) line with circles defines the minimum value of F where the spin is completely polarized, with SP = 1.

It is interesting to note that the minimum of F does not drop directly from the solid (red) line to the (black) line with circles with an increase in SP from 0 to 1. For instance, the pink line (with squares) and the purple line (with triangles) indicate the minimum value of F with SP = 0.177 and SP = 0.818,

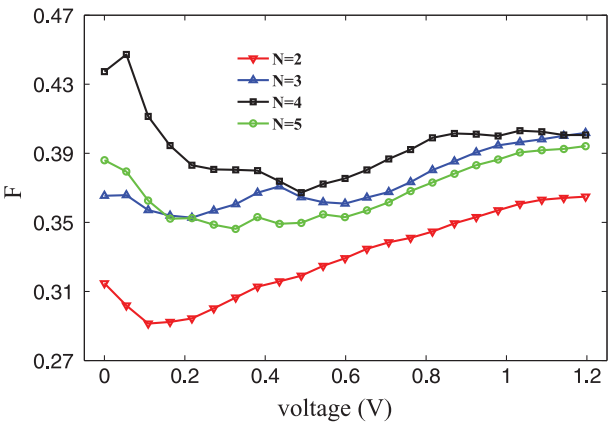

FIG. 5. (Color online) Fano factor versus bias voltage for Pt tunneling junctions with $N = 2$, 3, 4, and 5.

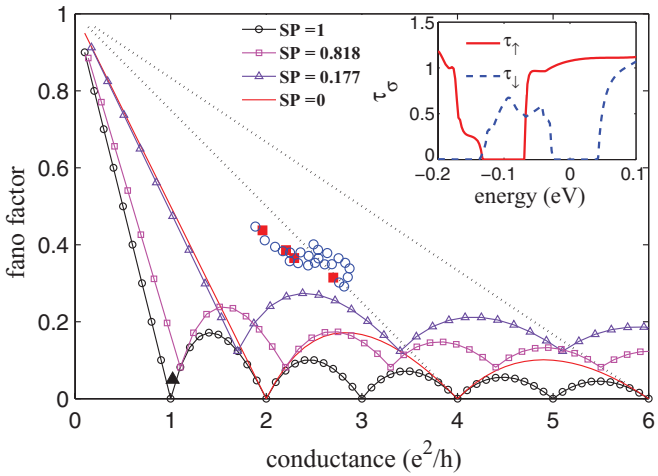

FIG. 6. (Color online) Fano factor versus differential conductance G for $N = 1,2,3,4$ under different bias voltages. Dotted lines indicate the maximum value of F for a system with four or six spin-degenerate eigenchannels. Filled (red) squares and open (blue) circles are, respectively, equilibrium and nonequilibrium values of F for Pt tunneling junctions. The triangle near $G = 1$ is the Fano factor of the 1D Pt tunneling junction. Inset: Transmission coefficient of the 1D Pt tunneling junction.

respectively. Obviously, all ofd the purple line is above the solid (red) line for almost all the conductance. This means that the Fano factor of a spin polarized configuration can be larger than the minimum value of F of the corresponding spin unpolarized configuration, and is not necessarily inside the region enclosed by the lines of the minimum of F with SP $= 0$ and SP $= 1$. Our numerical result confirms this point. In Fig. 6, we plot the Fano factor of all the Pt tunneling junctions when the bias voltage is close to 0 [filled (red) squares] and finite [open (blue) circles], respectively. We see that all points for the spin polarized configuration are above the solid (red) line. We wish to point out that our numerical value for the Fano factor is very close to the experimental data of Kummar *et al.*,[35] although their interpretation is different. To confirm our result further, we have calculated the Fano factor of a quasi-1D Pt magnetic tunneling junction where a Pt nanowire with four atoms is sandwiched between two semi-infinite quasi-1D Pt leads. The inset in Fig. 6 shows the spin polarized transmission coefficient of this structure. It shows that $\tau_\downarrow = 0$ and $\tau_\uparrow$ is around 1 at the Fermi level, which corresponds to the condition that SP $= 1$ and G is an odd number. In this case, F should be very close to 0, which is indeed consistent with our calculation, where the Fano factor is shown by the filled triangle in Fig. 6.

In summary, we have investigated the spin polarized transport properties and Fano factors of several Pt tunneling junctions. Our numerical results show that, roughly speaking, the current increases linearly with almost the same slope for all structures. In addition, the Fano factor shows sub-Poissonian behavior for all structures and bias voltages. In particular, we point out that the minimum Fano curve for an intermediate SP does not necessary lie between the minimum Fano curves for the unpolarized and fully polarized cases. Our numerical results confirm that the conductance of Pt atomic wires is spin polarized.

ACKNOWLEDGMENTS

We gratefully acknowledge the support from the Research Grant Council (Grant No. HKU 705409P) and University Grant Council (Contract No. AoE/P-04/08) of the Government of HKSAR.

*jianwang@hkusua.hku.hk

[1]For a review see N. Agrait, A. L. Yeyati, and J. M. van Ruitembeek, Phys. Rep. **377**, 81 (2003).
[2]H. Ohnishi, Y. Kondo, and K. Takayanagi, Nature **395**, 780 (1998).
[3]A. I. Yanson, G. Rubio Bollinger, H. E. van den Brom, N. Agraït, and J. M. van Ruitenbeek, Nature **395**, 783 (1998).
[4]B. H. Hong, S. C. Bae, C. W. Lee, S. Jeong, and K. S. Kim, Science **294**, 348 (2001).
[5]R. H. M. Smit, C. Untiedt, G. Rubio-Bollinger, R. C. Segers, and J. M. van Ruitenbeek, Phys. Rev. Lett. **91**, 076805 (2003).
[6]J. T. Wang, C. F. Chen, E. Wang, and Y. Kawazoe, Phys. Rev. Lett. **105**, 116102 (2010).
[7]P. C. Snijders and H. H. Weitering, Rev. Mod. Phys. **82**, 307 (2010).
[8]V. Rodrigues, J. Bettini, A. R. Rocha, L. G. C. Rego, and D. Ugarte, Phys. Rev. B **65**, 153402 (2002).
[9]J. L. Mozos, C. C. Wan, G. Taraschi, J. Wang, and H. Guo, Phys. Rev. B **56**, R4351 (1997).
[10]N. D. Lang and Ph. Avouris, Phys. Rev. Lett. **81**, 3515 (1998).
[11]H. S. Sim, H. W. Lee, and K. J. Chang, Phys. Rev. Lett. **87**, 096803 (2001).
[12]K. S. Thygesen and K. W. Jacobsen, Phys. Rev. Lett. **91**, 146801 (2003).
[13]F. Miao, D. Ohlberg, D. R. Stewart, R. S. Williams, and C. N. Lau, Phys. Rev. Lett. **101**, 016802 (2008).
[14]H. W. Yeom, S. Takeda, E. Rotenberg, I. Matsuda, K. Horikoshi, J. Schaefer, C. M. Lee, S. D. Kevan, T. Ohta, T. Nagao, and S. Hasegawa, Phys. Rev. Lett. **82**, 4898 (1999).
[15]A. Delin and E. Tosatti, Phys. Rev. B **68**, 144434 (2003).
[16]L. de la Vega, A. Martin-Rodero, A. Levy Yeyati, and A. Saúl, Phys. Rev. B **70**, 113107 (2004).
[17]J. Fernández-Rossier, D. Jacob, C. Untiedt, and J. J. Palacios, Phys. Rev. B **72**, 224418 (2005).
[18]N. Zabala, M. J. Puska, and R. M. Nieminen, Phys. Rev. Lett. **80**, 3336 (1998); **82**, 3000 (1999).
[19]V. A. Khlus, Sov. Phys. JETP **66**, 1243 (1987).
[20]M. Büttiker, Phys. Rev. Lett. **65**, 2901 (1990).
[21]M. Büttiker, Phys. Rev. B **46**, 12485 (1992).
[22]M. Reznikov, M. Heiblum, H. Shtrikman, and D. Mahalu, Phys. Rev. Lett. **75**, 3340 (1995).
[23]L. DiCarlo, Y. Zhang, D. T. McClure, D. J. Reilly, C. M. Marcus, L. N. Pfeiffer, and K. W. West, Phys. Rev. Lett. **97**, 036810 (2006).
[24]H. Birk, M. J. M. de Jong, and C. Schonenberger, Phys. Rev. Lett. **75**, 1610 (1995).

[25] A. Nauen, I. Hapke-Wurst, F. Hohls, U. Zeitler, R. J. Haug, and K. Pierz, Phys. Rev. B **66**, 161303(R) (2002).
[26] R. Danneau, F. Wu, M. F. Craciun, S. Russo, M. Y. Tomi, J. Salmilehto, A. F. Morpurgo, and P. J. Hakonen, Phys. Rev. Lett. **100**, 196802 (2008).
[27] R. Danneau, F. Wu, M. Y. Tomi, J. B. Oostinga, A. F. Morpurgo, and P. J. Hakonen, Phys. Rev. B **82**, 161405(R) (2010).
[28] H. E. van den Brom and J. M. van Ruitenbeek, Phys. Rev. Lett. **82**, 1526 (1999).
[29] V. V. Kuznetsov, E. E. Mendez, J. D. Bruno, and J. T. Pham, Phys. Rev. B **58**, 10159(R) (1998).
[30] S. S. Safonov, A. K. Savchenko, D. A. Bagrets, O. N. Jouravlev, Y. V. Nazarov, E. H. Linfield, and D. A. Ritchie, Phys. Rev. Lett. **91**, 136801 (2003).
[31] For a review see A. A. Clerk, M. H. Devoret, S. M. Girvin, F. Marquardt, and R. J. Schoelkopf, Rev. Mod. Phys. **82**, 1155 (2010).
[32] P. B. He and W. M. Liu, Phys. Rev. B **72**, 064410 (2005); Z. D. Li, J. Q. Liang, L. Li, and W. M. Liu, Phys. Rev. E **69**, 066611 (2004).
[33] Y. C. Chen and M. Di Ventra, Phys. Rev. B **67**, 153304 (2003); Phys. Rev. Lett. **95**, 166802 (2005).
[34] H. K. Zhao, L. L. Zhao, and J. Wang, Eur. Phys. J. B **77**, 441 (2010); Q. Zhang, D. Fu, B. G. Wang, R. Zhang, and D. Y. Xing, Phys. Rev. Lett. **101**, 047005 (2008).
[35] M. Kumar, O. Tal, R. H. M. Smit, and J. M. van Ruitenbeek, e-print arXiv:1101.3939v1 [cond-mat.mes-hall].
[36] P. Panigrahi and R. Pati, Phys. Rev. B **76**, 024431 (2007).
[37] B. G. Wang, J. Wang, and H. Guo, J. Phys. Soc. Jpn. **70**, 2645 (2001).
[38] P. X. Xu, V. M. Karpan, K. Xia, M. Zwierzycki, I. Marushchenko, and P. J. Kelly, Phys. Rev. B **73**, 180402(R) (2006).
[39] Y. D. Wei, B. G. Wang, J. Wang, and H. Guo, Phys. Rev. B **60**, 16900 (1999).
[40] G. Iannaccone, G. Lombardi, M. Macucci, and B. Pellegrini, Phys. Rev. Lett. **80**, 1054 (1998).
[41] P. Roche, J. Ségala, D. C. Glattli, J. T. Nicholls, M. Pepper, A. C. Graham, K. J. Thomas, M. Y. Simmons, and D. A. Ritchie, Phys. Rev. Lett. **93**, 116602 (2004).
[42] L. DiCarlo, Y. Zhang, D. T. McClure, D. J. Reilly, C. M. Marcus, L. N. Pfeiffer, and K. W. West, Phys. Rev. Lett. **97**, 036810 (2006).
[43] J. Taylor, H. Guo, and J. Wang, Phys. Rev. B **63**, 245407 (2001).
[44] The basic principle and practical implementation of the NEGF-DFT formalism to quantum transport can be found in Ref. 43. See also [http://www.nanoacademic.ca].
[45] L. Kleinman and D. M. Bylander, Phys. Rev. Lett. **48**, 1425 (1982).
[46] J. P. Perdew and Y. Wang, Phys. Rev. B **45**, 13244 (1992).